Effect of the change of the ancillary carboxylate bridging ligand on the SMM and luminescence properties of a series of carboxylate-diphenoxido triply bridged dinuclear ZnLn and tetranuclear Zn₂Ln₂ complexes (Ln = Dy, Er)†

E. Echenique-Errandonea,[a] A. Zabala-Lekuona,[a] J. Cepeda,[a] A. Rodríguez-Diéguez,[b]
J. M. Seco,[a] I. Oyarzabal*[c] and E. Colacio*[b]

Eleven new dinuclear and tetranuclear compounds of general formulae [Zn(μ-L)(μ-X)Ln(NO₃)₂]·nS, [Zn₂Dy₂(μ₃-L')₂(μ-sal)₂(NO₃)(CH₃OH)](NO₃)·5CH₃OH and [Zn₂Er₂(μ₃-L')₂(μ-sal)₂(CH₃OH)₂](NO₃)₂·4CH₃OH (X = benzoate, anthracenate, diclofenac, salicylate, 2,6-dihydroxybenzoate; Ln = Dy, Er; S = water, acetonitrile, methanol) were prepared from the *N,N'*-dimethyl-*N,N'*-bis(2-hydroxy-3-formyl-5-bromobenzyl) ethylenediamine compartmental ligand (H₂L). Complexes **1–6** and **9–11** consist of diphenoxido-carboxylate triply bridged compounds, which differ mainly in the carboxylate bridging ligand. It should be noted that the acidic character of the salicylic acid promotes, in the presence of methanol, the methoxylation of the H₂L ligand thereby yielding a hemiacetal H₃L', which is able to connect the Ln(III) ions of two ZnLn dinuclear units forming the Zn₂Ln₂ tetranuclear complexes **7** and **8**. All compounds display SMM behaviour in the presence of an external field with effective energy barriers (U_{eff}) as high as 61 K. Magneto-structural data for these complexes reveal that their SMM behaviour is not only significantly affected by the type of Ln(III) ion but also by the carboxylate bridging ligand connecting the Zn(II) and Ln(III) ions. Photoluminescence properties have also been accomplished, showing that the ligands are able to sensitize lanthanide centred emissions in the visible and near-infrared regions with variable capacity. Moreover, the analysis of the luminescence decay curves reveals emission lifetimes in the range of few microsecond or hundreds of nanoseconds for Dy(III)-based or Er(III)-based luminophores, respectively.

Introduction

Metal complexes that exhibit Single Molecule Magnet (SMM) behaviour (magnetic hysteresis below the so-called blocking temperature in the absence of polarizing field and slow relaxation for magnetization reversal) have been the target of many research efforts since their discovery in 1993.[1] The interest in

[a]Departamento de Química Aplicada, Facultad de Química, Universidad del País Vasco UPV/EHU, Paseo Manuel Lardizabal, no 3, 20018 Donostia-San Sebastián, Spain

[b]Departamento de Química Inorgánica, Facultad de Ciencias, Universidad de Granada, Av. Fuentenueva S/N, 18071 Granada, Spain. E-mail: ecolacio@ugr.es

[c]Centre de Recherche Paul Pascal, CNRS - Université de Bordeaux, 115 Avenue du Dr Albert Schweitzer, 33600 Pessac, France.

E-mail: oyarzabal@crpp-bordeaux.cnrs.fr

these nanomagnets is not surprising in view of the fascinating physical properties they exhibit, which could in principle be used for magnetic data storage[2] and molecular spintronics,[3] among other applications. Moreover, due to their quantum effects, SMMs could also be potentially applied in molecular quantum computing.[4]

Among the studied complexes, lanthanide-based compounds have resulted to be promising candidates for designing SMMs with improved properties, due to their large magnetic anisotropy.[5] These properties, together with high ground spin states, are tied to the existence of the energy barrier (U_{eff}) for the magnetization reversal, which is responsible for the SMM behaviour. In fact, energy barriers of up to 1815 K[6] and blocking temperatures (T_B) of around 60 K have been recently observed for Dy(III) based SMMs.[7]

In the past few years, our efforts have been focused on improving the magnetic properties of Dy(III) based SMMs by using the strategy of incorporating Zn(II) diamagnetic ions, which can attenuate the intermolecular magnetic interactions

that are responsible for the quantum tunnelling of magnetization (QTM), a shortcut for the magnetization reversal. The compartmental character of the H_2L ligand enables the encapsulation of two metallic centres which are interconnected by the carboxylate group of a second ligand, giving rise to a carboxylate-diphenoxido triple bridge between the Zn(II) and Dy(III) metal ions. As it has been suggested by theoretical and experimental studies, the coordination of the H_2L ligand to the Zn(II) ion can increase the electron density of the bridging phenoxido oxygen atoms, thus inducing a large electrostatic interaction with the Dy(III) ion.[8] As a consequence, the energy gaps between the crystal field levels of the Dy(III) ions are increased, leading to an enhancement of the U_{eff}.[8] On the other hand, the spatial arrangement of the oxygen donor atoms around the Dy(III) ions has a significant impact on the dynamic properties of Dy(III) SMMs, so that small changes such as the replacement of counteranions can lead to a great improvement of the energy barrier.[9]

In this paper, we would like to continue the study of the structural factors that modify the SMM properties of this kind of carboxylate-diphenoxido triply bridged Zn(II)–Ln(III) complexes. For this purpose, we have selected the already published [Zn(μ-L)(μ-OAc)Dy(NO$_3$)$_2$]·CH$_3$CN dinuclear complex, which exhibits an energy barrier of 41.55 K, as a reference point.[10] The aim is threefold: (i) to replace the acetate group by other bulkier carboxylate bridging ligands (benzoate, deprotonated diclofenac, salicylate and 9-anthracene carboxylate) which would lead to slight but significant modification of the Dy(III) coordination environment with the concomitant impact on the SMM properties, (ii) the further replacement of the Dy(III) ion by the Er(III) counterpart in all the complexes to know how the different shape of the electron density of the ground state of the Ln(III) ion (oblate and prolate for Dy(III) and Er(III), respectively) affects the SMM properties and (iii) finally, to study the ability of the compartmental and ancillary carboxylate ligands to act as an "antenna group" for sensitizing the characteristic emissions of Dy(III) and Er(III) compounds in the visible and near-infrared (NIR) regions, respectively. In particular, NIR luminescent complexes are of high interest due to their electronic and optical applications related to biomedicine,[11] encompassing their use as detectable immunoassays[12] or luminescent bio-thermometers,[13] especially when biocompatible molecules are employed.[14] In view of the above considerations, photoluminescence properties have also been studied in detail for all the reported complexes.

Experimental

Preparation of complexes

All reagents were obtained from commercial sources and used as received. The ligand H_2L was prepared following a reported procedure.[15]

[Zn(μ-L)(μ-OBz)Ln(NO$_3$)$_2$]·4CH$_3$OH·H$_2$O [Ln(III) = Dy (1), Er (2), OBz = benzoate]. 0.064 g (0.125 mmol) of H_2L, 0.125 mmol of the corresponding Ln(NO$_3$)$_3$·nH$_2$O and 0.018 g (0.125 mmol)

of NaOBz were successively added under continuous stirring to a solution of 0.033 g (0.125 mmol) of Zn(NO$_3$)$_2$·4H$_2$O in 5 mL of methanol. The solution was stirred for 30 minutes, filtered to eliminate any amounts of insoluble materials and the filtrate was kept undisturbed at room temperature for several days, whereupon yellow X-ray quality crystals were obtained. Yield: 30% for **1** and 29% for **2**. Anal. calcd for C$_{31}$H$_{43}$Br$_2$DyN$_4$O$_{17}$Zn: C, 32.91; H, 3.83; N, 4.95. Found: C, 32.45; H, 3.86; N, 5.04. Anal. calcd for C$_{31}$H$_{43}$Br$_2$ErN$_4$O$_{17}$Zn: C, 32.77; H, 3.81; N, 4.93. Found: C, 32.83; H, 3.84; N, 5.00.

[Zn(μ-L)(μ-9-An)Ln(NO$_3$)$_2$]·CH$_3$CN [Ln(III) = Dy (3), Er (4), 9-An = 9-anthracenecarboxylate]. To a solution of 0.033 g (0.125 mmol) of Zn(NO$_3$)$_2$·4H$_2$O in 5 mL of acetonitrile were subsequently added 0.064 g (0.125 mmol) of H_2L and 0.125 mmol of the corresponding Ln(NO$_3$)$_3$·nH$_2$O under continuous stirring. To the resulting solution was then added dropwise another solution containing 0.028 g (0.125 mmol) of 9-anthracenecarboxylic acid and 0.038 g (0.375 mmol) of Et$_3$N in 5 mL of acetonitrile, leading to the formation of a yellow precipitate. The powder was collected by filtration and dried under vacuum (yields: 62 and 54% for **3** and **4**, respectively), while the solution was left undisturbed at room temperature for several days, affording crystals of **3** and **4.** The powdered and crystalline samples were proved to be the same by X-ray diffraction (Fig. S3†). Yield of crystals: 13% for **3** and 17% for **4**. Anal. calcd for C$_{37}$H$_{32}$Br$_2$DyN$_5$O$_{12}$Zn: C, 39.46; H, 2.86; N, 6.22. Found: C, 39.61; H, 2.87; N, 6.26. Anal. calcd for C$_{37}$H$_{32}$Br$_2$ErN$_5$O$_{12}$Zn: C, 39.29; H, 2.85; N, 6.19. Found: C, 39.30; H, 2.87; N, 6.20.

[Zn(μ-L)(μ-dicl)Ln(NO$_3$)$_2$]·H$_2$O [Ln(III) = Dy (5), Er (6), dicl = deprotonated diclofenac = 2-[(2,6-dichlorophenyl)amino] benzene acetate]. These compounds were synthesised following the same procedure as that for **1** and **2**, but using diclofenac sodium salt (0.040 g, 0.125 mmol) instead of NaOBz. Yield: 42% for **5** and 48% for **6**. Anal. calcd for C$_{34}$H$_{32}$N$_5$O$_{13}$Br$_2$Cl$_2$DyZn: C, 34.69; H, 2.74; N, 5.95. Found: C, 34.81; H, 2.75; N, 5.96. Anal. calcd for C$_{34}$H$_{32}$N$_5$O$_{13}$Br$_2$Cl$_2$ErZn: C, 34.55; H, 2.73; N, 5.92. Found: C, 34.61; H, 2.74; N, 5.90.

[Zn$_2$Dy$_2$(μ$_3$-L′)$_2$(μ-sal)$_2$(NO$_3$)(CH$_3$OH)]NO$_3$·5CH$_3$OH [7, sal = salicylate]. 0.064 g (0.125 mmol) of H_2L, 0.055 g (0.125 mmol) of Dy(NO$_3$)$_3$·5H$_2$O and 0.033 g (0.125 mmol) of Zn(NO$_3$)$_2$·4H$_2$O were dissolved in 10 mL of hot methanol (60 °C). To this solution was added dropwise another solution containing 0.017 g (0.125 mmol) of salicylic acid and 0.050 g (0.5 mmol) of Et$_3$N in 5 mL of methanol. The yellow solution was stirred for 15 minutes while heating, filtered and the filtrate was kept undisturbed at room temperature so that yellow crystals were obtained. After filtration, the compound exhibited a phase transformation due to the loss of 3 crystallization molecules, as deducted from the thermogravimetric measurements (Fig. S9†). Yield: 33%. Anal. calcd for C$_{59}$H$_{68}$Br$_4$Dy$_2$N$_6$O$_{25}$Zn$_2$ (only 2 crystallization methanol molecules were considered): C, 34.80; H, 3.37; N, 4.13. Found: C, 34.66; H, 3.32; N, 4.19.

[Zn$_2$Er$_2$(μ$_3$-L′)$_2$(μ-sal)$_2$(CH$_3$OH)$_2$](NO$_3$)$_2$·4CH$_3$OH [8, sal= salicylate]. This complex was prepared following the same procedure as that for **7**, but using Er(NO$_3$)$_3$·5H$_2$O (0.055 g,

0.125 mmol) instead of Dy(NO$_3$)$_3$·5H$_2$O. A phase transformation was also observed in this compound, which led to the loss of 2 methanol molecules (Fig. S10†). Yield: 28%. Anal. calcd forC$_{60}$H$_{72}$Br$_4$Er$_2$N$_6$O$_{26}$Zn$_2$ (only 2 crystallization methanol molecules were considered): C, 34.68; H, 3.49; N, 4.04. Found: C, 34.55; H, 3.52; N, 4.13.

[Zn(μ-L)(μ-sal)Ln(NO$_3$)$_2$]·2CH$_3$CN [Ln(III) = Dy (9), Er (10), sal = salicylate]. To a solution of 0.033 g (0.125 mmol) of Zn(NO$_3$)$_2$·4H$_2$O in 5 mL of acetonitrile were subsequently added 0.064 g (0.125 mmol) of H$_2$L and 0.125 mmol of the corresponding Ln(NO$_3$)$_3$·nH$_2$O under continuous stirring. To the resulting solution was then added dropwise another solution containing 0.017 g (0.125 mmol) of salicylic acid and 0.050 g (0.500 mmol) of Et$_3$N in 5 mL of acetonitrile. The obtained yellow solution was stirred for 30 minutes, filtered and the filtrate was kept undisturbed at room temperature for several days, whereupon yellow X-ray quality crystals were obtained. Yield: 64% for **9** and 73% for **10**. Anal. calcd for C$_{31}$H$_{30}$Br$_2$DyN$_6$O$_{13}$Zn: C, 34.40; H, 2.79; N, 7.76. Found: C, 34.68; H, 2.87; N, 7.72. Anal. calcd for C$_{31}$H$_{30}$Br$_2$ErN$_6$O$_{13}$Zn: C, 34.25; H, 2.78; N, 7.73. Found: C, 34.50; H, 2.72; N, 7.76.

[Zn(μ-L)(μ-2,6-dihydbenz)Er(NO$_3$)$_2$]·2CH$_3$CN [11, 2,6-dihydbenz = 2,6-dihydroxybenzoate]. To a hot solution (80 °C) of 0.064 g (0.125 mmol) of H$_2$L in 7 mL of acetonitrile were added 0.033 g (0.125 mmol) of Zn(NO$_3$)$_2$·4H$_2$O and 0.055 g (0.125 mmol) of Er(NO$_3$)$_3$·5H$_2$O. Then, a solution containing 0.019 g (0.125 mmol) of 2,6-dihydroxybenzoic acid and 0.050 g (0.500 mmol) of Et$_3$N in 5 mL of acetonitrile was added. The resulting yellow solution was stirred for 30 minutes while heating, filtered to eliminate any amount of insoluble material and the filtrate was kept undisturbed at room temperature. In few days, X-ray quality crystals of **11** were obtained. Yield 80%. Anal. calcd for C$_{31}$H$_{31}$Br$_2$ErN$_6$O$_{14}$Zn: C, 33.72; H, 2.83; N, 7.61. Found: C, 33.93; H, 2.89; N, 7.73.

In addition to the elemental analyses, the purity of all the samples was checked by powder X-ray diffraction (Fig. S2–S8, ESI†).

Physical measurements

Elemental analyses (C, H and N) were carried out at the Centro de Instrumentación Científica (University of Granada) on a Fisons-Carlo Erba analyzer model EA 1108 (Thermo Scientific, Waltham, MA, USA). Infrared (IR) spectra (400–4000 cm^{-1}) were recorded on a Nicolet FT-IR 6700 spectrometer in KBr pellets. Powder X-ray diffraction (PXRD) patterns were collected on a Phillips X'PERT powder diffractometer with Cu Kα radiation (λ = 1.5418 Å) over the range $5 \leq 2\theta \leq 50°$ with a step size of 0.026° and acquisition time of 2.5 s per step at 25 °C. Thermal analyses (TG/DTA) were performed on a TA Instruments SDT 2960 thermal analyser under a synthetic air atmosphere (79% N$_2$/21% O$_2$) with a heating rate of 5 °C min^{-1}. Alternating current (*ac*) magnetic measurements were recorded on a PPMS (Physical Property Measurement System) – Quantum Design Model 6000 magnetometer using 60 to 10 000 Hz frequencies. Lifetime and steady-state photoluminescence (PL) measurements were carried out on crystal-

line samples from 10 K to room temperature using a close cycle helium cryostat enclosed in an Edinburgh Instruments FLS920 spectrometer. For recording steady-state emission spectra an IK3552R-G HeCd continuous laser (325 nm) was used as an excitation source and a Hamamatsu NIR-PMT PicoQuant FluoTime 200 detector, whereas a Müller-Elektronik-Optik SVX1450 Xe lamp was employed to collect the excitation spectra.

Single-crystal structure determination

Single crystals of suitable dimensions were used for data collection. For compound **1**, diffraction intensities were collected on an Agilent Technologies Super-Nova diffractometer, which was equipped with monochromated Cu Kα radiation (λ = 1.54184 Å) and an Atlas CCD detector at 100(2) K. The intensity data for compounds **2–4** and **10** were also collected on an Agilent Technologies Super-Nova diffractometer, but equipped with monochromated Mo Kα radiation (λ = 0.71073 Å) and an Eos CCD detector. In all cases, data frames were processed (unit cell determinations, intensity data integrations, routine corrections for Lorentz and polarization effects and analytical absorption corrections) using the CrysAlis Pro software package.[16] The intensity data for compounds **5–8** and **11** were collected on a Bruker SMART APEX CCD area diffractometer (Bruker, Billerica, MA, USA) using monochromated Mo Kα radiation (λ = 0.71073 Å). The data reduction was performed with the APEX2[17] software and corrected for absorption using SADABS.[18] In all cases, the structures were solved by direct methods and refined by full-matrix least-squares with SHELXL-2014.[19]

During the refinement of complexes **1** and **2**, most of the lattice solvent molecules were found to be largely disordered, which did not allow inferring the hydrogen bonding scheme. Therefore, these structures were refined with a new set of F^2 (*hkl*) values without the contribution from solvent molecules obtained by the SQUEEZE procedure as implemented in PLATON-v1.18.[20] The same procedure was followed for **5**, **6** and **10** given the disordered arrangement of crystallization solvent molecules, which despite allowing to identify their amount and nature could not be correctly refined. On the other hand, one lattice acetonitrile molecule crystallized in the structure of **11** is slightly disordered with its nitrogen atom occurring at two positions with 70% and 30% relative occupancies. On the other hand, during the last refinements of the structures of **3** and **4**, unusually high error factors were found, suggesting the occurrence of twinning. Accordingly, (0.557 0.139 −0.446/0 −1 −0/−1.549 −0.137 −0.555) twin law was applied to integrate diffraction data, which led to a substantial decrease of the agreement factors. Percentages of *ca.* 44 and 50% were obtained for the minor domain of crystals of **3** and **4**, respectively. Final $R(F)$, w$R(F^2)$ and goodness of fit agreement factors, details of data collection and analyses can be found in Table S1.† Selected bond lengths and angles are given in Table S2.† Ortep views of all compounds are shown in Fig. S11–S15.† CCDC reference numbers for the structures are 1858756–1858765.†

Results and discussion

The flexible polytopic ligand H$_2$L allowed the formation of several Zn(II)–Ln(III) dinuclear complexes by varying the ancillary carboxylate bridging ligand as well as the reaction conditions (Fig. 1). Thus, the reaction of the H$_2$L ligand with Zn(NO$_3$)$_2$·4H$_2$O, Ln(NO$_3$)$_3$·nH$_2$O and the corresponding carboxylate ancillary ligand in either methanol or acetonitrile with a 1 : 1 : 1 : 1 molar ratio afforded the dinuclear complexes **1–6**. For **1**, **2**, **5** and **6** the sodium salts of the benzoic (NaOBz) and diclofenac (Nadicl) acids, respectively, were used as sources of carboxylate anions and methanol as the solvent, whereas for 3 and **4** the 9-anthracene carboxylate anion (9-An) was prepared *in situ* from the reaction of 9-An acid with Et$_3$N in acetonitrile. Finally, what is more interesting is that the use of salicylic acid under the same reaction conditions as those for **1–2** and **5–6** led to the formation of the tetranuclear Zn$_2$Ln$_2$ complexes **7** and **8**, in which one of the two formyl groups of the H$_2$L ligand is transformed into a hemiacetal group, leading to the H$_3$L′ ligand (Fig. 2). The methoxylation process observed in **7** and **8** is promoted by the acidic character of the salicylic acid, which is necessary to undergo this type of reaction.[21] In complexes **1–2** and **5–6**, which were prepared using basic sodium salts, and in complexes **3** and **4**, which were obtained using acetonitrile as the solvent, the formation of the hemiacetal does not occur. In order to gain insight into the mentioned process, the reactions of complexes **7** and **8** were repeated in acetonitrile, which gave rise, as expected, to single crystals of dinuclear Zn(II)–Ln(III) species (complexes **9** and **10**). Finally, it should be noted that the same process was already observed in the tetranuclear Cu$_2$Gd$_2$ complex with the general formula {[CuGd(L′)(OAc)(H$_2$O)]ClO$_4$·3.5CH$_3$OH}$_2$, which differs from **7**
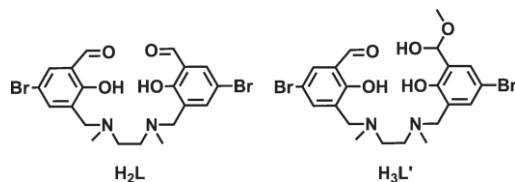
Fig. 2 Schematic view of ligands H$_2$L and H$_3$L′.

and **8** in the bridging carboxylate group (acetate instead of salicylate).[22]

Crystal structures

Compounds **1** and **2** are isostructural and consist of Zn(II)–Ln(III) dinuclear species that crystallize in the *C2/c* space group, in which Zn(II) and Ln(III) ions are triply bridged by two diphenoxido groups belonging to the L^{2-} ligand and a *syn–syn* benzoate ligand (Fig. 1). The Zn(II) ion is also coordinated to the two nitrogen atoms of the L^{2-} ligand, whereas the LnO$_9$ coordination sphere is completed by the additional coordination of the two aldehyde oxygen atoms belonging to the L^{2-} ligand and four oxygen atoms from the two bidentate nitrate anions. The ZnN$_2$O$_3$ coordination sphere is best described as a square pyramid, while the lanthanide ions show a geometry that is close to the spherical capped square antiprism according to continuous-shape-measures (CShMs) using SHAPE software (Tables S3 and S4†).[23] The dinuclear entities of **1** and **2** are surrounded by disordered lattice methanol and water molecules, which are involved in hydrogen bonding interactions giving rise to an intricate supramolecular network (see Fig. S16 in the
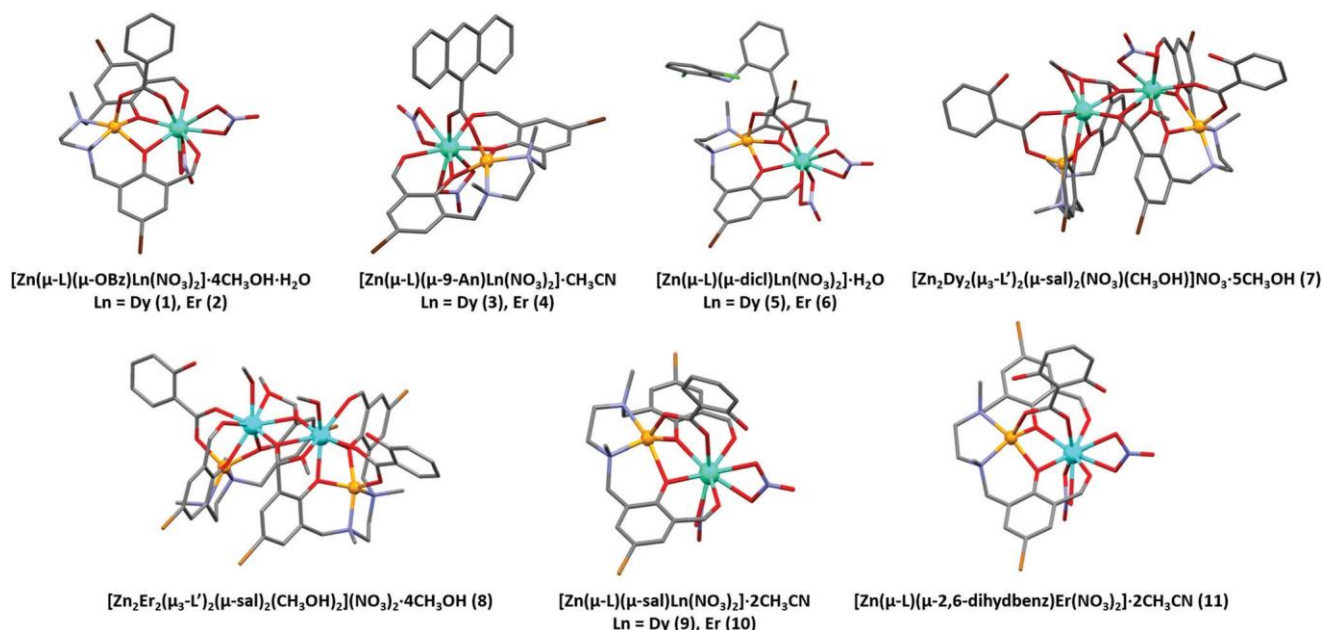
[Zn(μ-L)(μ-OBz)Ln(NO$_3$)$_2$]·4CH$_3$OH·H$_2$O
Ln = Dy (1), Er (2)

[Zn(μ-L)(μ-9-An)Ln(NO$_3$)$_2$]·CH$_3$CN
Ln = Dy (3), Er (4)

[Zn(μ-L)(μ-dicl)Ln(NO$_3$)$_2$]·H$_2$O
Ln = Dy (5), Er (6)

[Zn$_2$Dy$_2$(μ$_3$-L′)$_2$(μ-sal)$_2$(NO$_3$)(CH$_3$OH)]NO$_3$·5CH$_3$OH (7)

[Zn$_2$Er$_2$(μ$_3$-L′)$_2$(μ-sal)$_2$(CH$_3$OH)$_2$](NO$_3$)$_2$·4CH$_3$OH (8)

[Zn(μ-L)(μ-sal)Ln(NO$_3$)$_2$]·2CH$_3$CN
Ln = Dy (9), Er (10)

[Zn(μ-L)(μ-2,6-dihydbenz)Er(NO$_3$)$_2$]·2CH$_3$CN (11)

Fig. 1 Perspective views of the structures of **1–11**. Colour code: N = blue, O = red, C = gray, Br = brown, Cl = green, Zn = light brown, Ln = turquoise. H atoms, counteranions and crystallization solvent molecules have been omitted for the sake of clarity.

ESI†). The large disorder present in those molecules precludes describing the intermolecular interactions in detail.

The structures of compounds 3–6 are similar to those of 1 and 2, but they contain either 9-anthracenecarboxylate (3 and 4) or diclofenac (5 and 6) instead of benzoate as the ancillary *syn−syn* carboxylate bridging ligand. Continuous-shape-measures (CShMs) indicate that the change of this latter ligand leads to small differences in their structures, as well as in the coordination environments of the metal ions. Ln−O_{ligand} distances are almost identical in complexes 1 and 5, as well as in 2 and 6, and are in the 2.306–2.380 Å range. The Ln···$O_{carboxylate}$ and Zn···Ln distances are slightly longer in the benzoate bridged compounds than in the diclofenac counterparts (in the 2.264–2.291 and 3.353–3.376 Å ranges, respectively), whereas the Zn···$O_{carboxylate}$ bond distances (between 1.957 and 1.977 Å) follow the opposite trend. The Zn−O_{ligand} and Zn−N bond distances are respectively in the 2.063–2.131 and 2.095–2.130 Å ranges in these four compounds, and the lowest Ln···Ln distance is of 8.2 Å.

It is worth noting that complexes 3 and 4 contain two different dinuclear molecules, which show slightly different bond lengths and angles. Although most of the bond distances follow a similar trend to that observed for the previously described complexes, Zn−$O_{carboxylate}$ and Ln−$O_{carboxylate}$ bond distances (in the 1.981−1.997 and 2.303−2.327 Å ranges, respectively) are larger in the anthracenate containing compounds (3 and 4) than in complexes 1, 2, 5, and 6. Despite the bulkier bridging groups, the lowest Ln···Ln distances are shorter in 3 and 4 (of 7.675 and 7.673 Å, respectively) than those observed in the benzoate and diclofenac containing compounds. Compounds 3–6 present significant differences with regard to the supramolecular interactions which build up their packing compared to that of 1–2. Unlike hydrogen bonding interactions governing the crystal building of 1–2, packing of 3–6 is governed by π···π interactions. In particular, the voluminous aromatic rings of the 9-anthracenecarboxylate ligand promote strong face-to-face contacts among consecutive dimeric entities (see Fig. S16†). On the other hand, the bulkier and more twisted nature of the aromatic rings of the diclofenac ligand only allows establishing less intense C−H··· π interactions among neighbouring dimeric molecules (Fig. S17†).

As discussed before, complexes 7 and 8 show different structures to 1–6. Specifically, in these compounds one of the carbonyl groups of the H_2L ligand is transformed into a hemiacetal group when reacted with the methanol solvent. This reaction leads to a new ligand, H_3L', with a larger denticity coordination mode, which is able to form tetranuclear complexes where the Ln(III) ions of Zn(II)−Ln(III) dinuclear units are connected by the alkoxy and methoxy groups of the hemiacetal moiety. Although ZnN_2O_3 chromophores are not greatly affected after the coordination of the *in situ* generated L'^{3-} ligand, the coordination environments of the lanthanide ions (there are two crystallographically independent Ln(III) ions, Ln1 and Ln2) undergo significant changes compared to complexes 1–6. In fact, in complex 7, the Dy1 ion exhibits a LnO_9 coordination sphere, which is formed by the binding of

one methoxy group, one alkoxido-bridge (connecting Dy1 and Dy2 ions), one aldehyde, two phenoxido oxygen atoms belonging to a L'^{3-} ligand, one alkoxo-bridging oxygen atom pertaining to another L'^{3-} ligand, one oxygen atom from the salicylate bridging ligand bridging the Zn(II) and Dy(III) and one biden-tate nitrate anion. In contrast, the LnO_8 coordination environ-ment of the Dy2 atom is formed by the coordination of a methanol molecule instead of a bidentate nitrate anion. The coordination spheres of Dy1 and Dy2 are best described as the spherical tricapped trigonal prism and biaugmented trigonal prism, respectively, according to SHAPE measurement results (Tables S4 and S5†). In complex 8, Er1 exhibits a similar coordination environment to that observed for Dy1 in complex 7, in which the bidentate nitrate ion is replaced by a co-ordinated methanol molecule, leading to a LnO_8 configuration.

In addition, Er2 displays the same LnO_8 coordination environment as Dy2 in complex 7. The coordination spheres of Er1 and Er2 are best described as a triangular dodecahedron according to SHAPE measurement results (Table S5†). It is important to note that in these compounds, the tetranuclear entities are weakly bonded to each other by either Br···π contacts or hydrogen bonding interactions involving both lattice methanol and nitrate anions, some of which consist of negligible C−H···O contacts (Fig. S17 and S18†). Probably as a consequence of the lack of cohesion in the packing, compounds 7 and 8 undergo rapid phase transformations (as revealed by their PXRD data, see Fig. S5 and S6†) when single crystals are removed from mother liquids, a fact that does not bring any significant change in the structures of the molecules but a mere partial loss of lattice solvent molecules (see Fig. S9 and S10†).

As mentioned above, dinuclear complexes with salicylate as the bridging ligand can also be obtained by changing the reaction conditions. In these complexes (9 and 10), the phenol group of the salicylate ligand is disordered in such a way that it is able to form hydrogen bonding interactions with both oxygen atoms of the bridging carboxylate group (Fig. 3). Finally, in order to evaluate the contribution of the disordered phenol group to magnetic properties, compound 11 was synthesized using 2,6-dihydroxybenzoate as the bridging ligand. In this compound, both phenol groups establish hydrogen
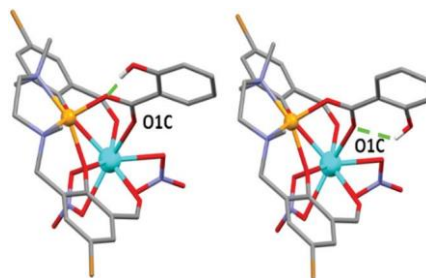

Fig. 3 Hydrogen bond interactions between the phenol group and one of the oxygen atoms belonging to the carboxylate group of the salicylate ligand.

bonds with the carboxylate group and consequently there is no disorder. This leads to structurally and magnetically equivalent Er(III) ions as they receive the same electron density from the ligands. Due to the similarity with the previous dinuclear complexes, no further comments are required. To end up with the structural description, it is worth mentioning that crystal packing of compounds **9–11** grows from lateral π···π interactions between the aromatic rings of salicylate/2,6-dihydroxybenzoate and L ligands, while weak Br···π contacts reinforce the packing robustness (Fig. S18 and S19†).

Magnetic properties

Regarding the magnetic properties, alternate current (*ac*) magnetic measurements only revealed a slight frequency dependency of the χ''_M signals for **1** and **3**, but without any clear maximum above 2 K (Fig. S20 and S21†). As the observed behaviour could be due to the existence of QTM, the measurements were repeated in the presence of an external field of 1000 Oe in order to remove it (this is the optimal field that produces the highest relaxation time), obtaining frequency dependent signals for all complexes (Fig. 4, 5 and S22–S30†). However, compounds **7** and **9** continue showing weak frequency dependent signals in χ''_M *vs.* *T* plots (Fig. S26 and S28†).

For complexes **1**, **2**, **4–6** and **8**, the temperature dependence of χ''_M at each frequency was fitted to the generalized Debye
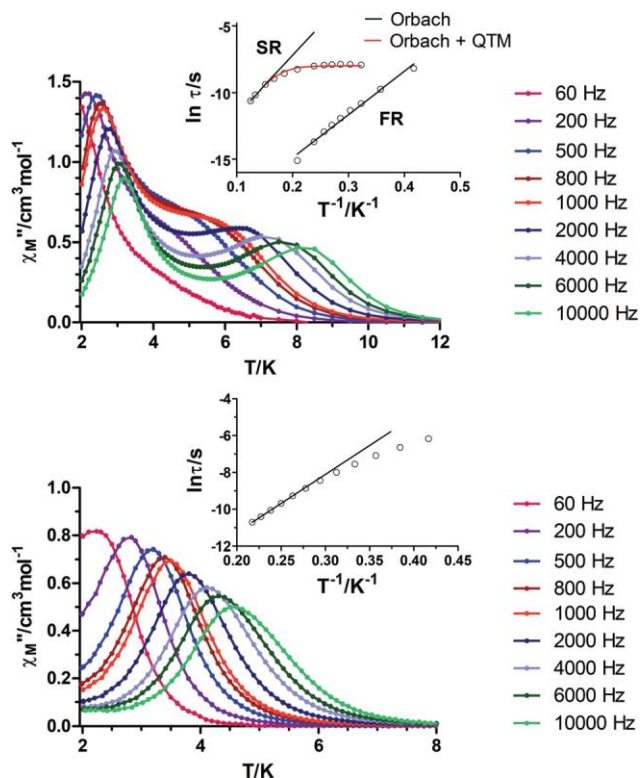

Fig. 4 Temperature dependence of out-of-phase components of the *ac* susceptibility in a *dc* applied field of 1000 Oe for **3** (up) and **4** (bottom). Inset: Arrhenius plots for **3** (up) and **4** (bottom). The black line accounts for the best fit considering Orbach relaxation, and the red line corresponds to Orbach plus QTM relaxation.
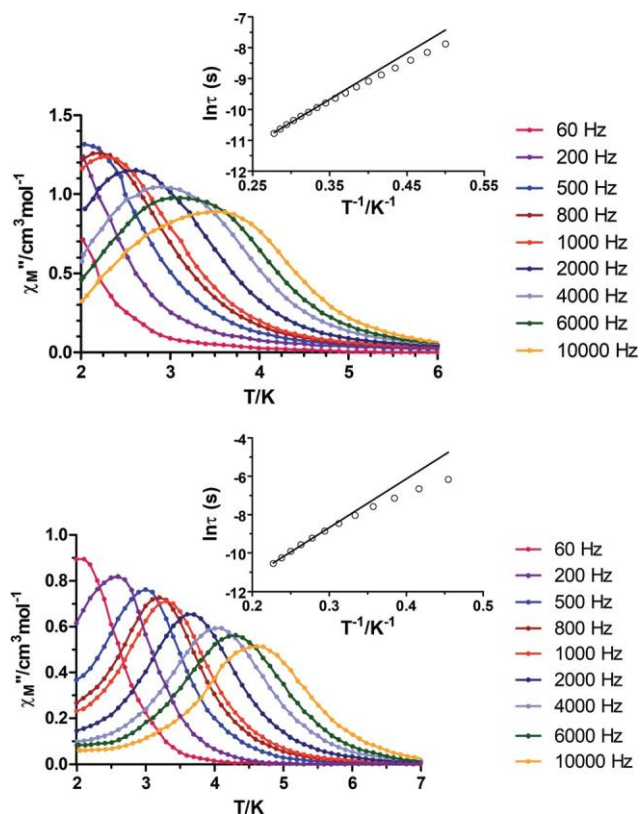

Fig. 5 Temperature dependence of out-of-phase components of the *ac* susceptibility in a *dc* applied field of 1000 Oe for **5** (up) and **6** (bottom). Insets: Arrhenius plots for **5** (up) and **6** (bottom). The black line accounts for the best fit considering the Orbach relaxation mode.

model, obtaining relaxation times at different temperatures (Fig. 4, 5, S22 and S26,† insets). The linear portion of the data was then fitted to the Arrhenius equation, leading to the effective energy barrier (U_{eff}) and τ_0 values that are indicated in Table 1. The deviation of the relaxation times from linearity suggests that, besides the Orbach relaxation mode, other relaxation pathways are also present at low temperatures. This conclusion is also supported by the α values accomplished from the Cole–Cole plots, which deviate significantly from 0 at the lowest temperatures (Fig. S32–S35†).

Even though an external *dc* field was applied for compound **8**, χ'_M and χ''_M components do not go to zero below the maxima. This effect, in addition to the temperature-independent ln τ values below 2.8 K (Fig. S26,† inset), indicates that the QTM effect was not completely quenched. Therefore, the data were fitted to the simultaneous presence of Orbach and QTM mechanisms using eqn (1). The extracted values for U_{eff}, τ_{QTM} and τ_0 are listed in Table 1.

$$\tau^{-1} = \tau_{QTM}^{-1} + \tau_0^{-1} \exp(-U_{eff}=k_BT) \tag{1}$$

In the case of complex **3**, two different maxima in the χ'_M and χ''_M *vs.* *T* plots were observed in the temperature ranges 2.0 K–3.5 K and 5.0–8.5 K for the fast (FR)- and slow (SR)-relaxation processes, respectively (Fig. 4 and S24†). Both processes

Table 1 U_{eff}, τ_0 and τ_{QTM} values for complexes **1–6**, **8**, **10** and **11**

Comp.	Orbach		Orbach + QTM		
	U_{eff} (K)	τ_0 (s)	U_{eff} (K)	τ_0 (s)	τ_{QTM} (s)
1	61.5	9.64×10^{-9}			
2	18.0	2.03×10^{-7}			
3	32.4 FR	5.26×10^{-10} FR	52.8 SR	3.62×10^{-8}	3.32×10^{-4}
	45.1 SR	9.00×10^{-8} SR			
4	31.4	2.44×10^{-8}			
5	15.0	3.35×10^{-7}			
6	25.4	8.35×10^{-8}			
8	25.8	3.35×10^{-8}	40.1	1.09×10^{-9}	1.09×10^{-4}
10	9.6 FR	6.20×10^{-7} FR			
	17.3 SR	7.87×10^{-7} SR			
11	24.0	1.19×10^{-7}			

can be also observed in the Cole–Cole plots (Fig. S33†) in the 3.1–3.9 K range, where a combination of semicircles appears. The data were fitted by using a sum of two modified Debye functions with the CCFIT Software[24] and relaxation times for both processes were extracted (Table S6†). Arrhenius plots were constructed for both relaxation processes (Fig. 4, inset) in the high-temperature region, affording effective energy barriers for the reversal of the magnetization and τ_0 values of 32.4 K with $\tau_0 = 5.26 \times 10^{-10}$ s and 45.1 K with $\tau_0 = 9.00 \times 10^{-8}$ s for FR and SR, respectively. However, in the case of the SR, relaxation times at lower temperatures deviate from linearity, which could be due to the presence of other relaxation processes that are not thermally activated. Hence, the data were fitted again to eqn (1) obtaining the following new parameters: $U_{\text{eff}} = 52.8$ K, $\tau_0 = 3.62 \times 10^{-8}$ s and $\tau_{\text{QTM}} = 3.32 \times 10^{-4}$ s.

It is worth mentioning at this point that the observation of two maxima in the temperature and frequency dependence of χ'_{M} and χ''_{M} plots can be explained by the existence of two crystallographically independent Dy(III) ions in the asymmetric unit of the crystal structure, as already discussed above and as it was previously shown in the literature.[25] Nevertheless, it should be remarked that two maxima have also been found for compounds containing only one independent crystallographic Dy(III) ion.[26] In some cases, the relaxation process at lower temperatures has been suggested to be due to: (i) a direct process arising from the multi-level system due to the lifting of the Kramers degeneracy of the Ln(III) ground state by the static magnetic field and (ii) intermolecular interactions.[27] All these considerations point out the complexity of the relaxation process in lanthanide(III) complexes. At variance with complex **3**, the isostructural Er(III) counterpart (**4**) does not present two differentiated relaxation processes. This fact seems to indicate that: (i) the existence of two crystallographically independent Dy(III) ions in **3** could not be the reason for the observation of two well separated relaxation processes for this compound and (ii) the relaxation process appearing at lower temperatures in **3** could not arise from intermolecular interactions. The dynamic analysis of diluted sample Y/Dy = 10/1 of compound **3** reveals no significant difference between the *ac* properties of the pristine compound **3** and its diluted complex, thus ruling out the

intermolecular origin of the process occurring at lower temperatures (Fig. S31†). Therefore, both relaxation processes observed for **3** should be single-ion in origin and, moreover, the existence of two crystallographically independent Ln(III) ions should not be the reason for the observation of two relaxation processes, as their maxima should appear very close in the temperature and frequency dependence of χ'_{M} and χ''_{M} plots, so that they could not be discriminated. The fact that **4** does not exhibit the relaxation process appearing at lower temperature in **3** could be ascribed to the different structure of the energy levels between Dy(III) and Er(III) ions in these complexes.

Additionally, complex **10** also exhibits two maxima in χ'_{M} and χ''_{M} vs. *T* plots (Fig. S28 and S29†). The peak appearing at higher temperature could be due to a thermally activated process, whereas the one occurring at lower temperature could have their origin, as for complex **3**, in: (i) a direct process arising from the multi-level system due to the lifting of the Kramers degeneracy of the Ln(III) ground state by the static magnetic field, (ii) intermolecular interactions and (iii) the disordered phenol group of the salicylate ligand could give rise to two chemically independent molecules depending on the position of the phenol group (Fig. 3). Thus, the hydrogen atom of the phenol group could form hydrogen bonds with each of the carboxylate oxygen atoms of the salicylate ligand, so that the charge that the Er(III) ion receives from O1C would be different if the hydrogen bond is established with the carboxylate oxygen atom bonded to the Zn(II) ion or with that bonded to the Er(III) ion. These two conformations could lead to two Er(III) with different electronic density environments, which could cause the appearance of two peaks in the temperature and frequency dependence of the out-of-phase *ac* magnetic susceptibility plots. The fact that complex **2**, which contains a benzoate bridging group that cannot form hydrogen bonds, presents only one relaxation process could support this suggestion. The two maxima in the χ''_{M} vs. *T* plot for complex **10** appear in the 2.0–3.0 K and 4.0–5.0 K temperature range, which correspond to the fast (FR)- and slow (SR)-relaxation processes, respectively. Both processes can be observed as well in the Cole–Cole plots (Fig. S35†) in the 2.0–3.2 K range, where

a combination of two semicircles is appreciable. The data were fitted to a sum of two modified Debye functions using the CCFIT software affording relaxation times for both processes (Table S7†). Arrhenius plots were constructed for both relaxation processes (Fig. S28,† inset) in the high-temperature region and the fit afforded effective energy barriers for the reversal of the magnetization of 9.6 K with $\tau_0 = 6.20 \times 10^{-7}$ s and 17.3 K with $\tau_0 = 7.87 \times 10^{-7}$ s for FR and SR, respectively.

In order to support the above-mentioned hypothesis, we prepared compound **11**, which contains 2,6-dihydroxybenzoate as the ancillary bridging ligand. The two phenol groups of this ligand are symmetrically located at both sides of the carboxylate bridging group, so that, as indicated elsewhere, they form simultaneously hydrogen bonds with the carboxylate oxygen atoms. These symmetrical interactions are not compatible with the existence of two magnetically independent Er(III) ions in the sample. The χ'_M and χ''_M vs. T plots (Fig. S30†), as well as the Cole–Cole plots (Fig. S36†), are in good agreement with this suggestion, as a single maximum is observed in the in-phase and out-of-phase susceptibility plot, as well as a single semicircle in the Cole–Cole plots, in contrast to what occurs for compound **10**. However, these results should be taken with care. Even though the disordered hydrogen bond in compound **10** could be responsible for the slight change of the electron density around the Er(III) ion leading virtually to two magnetically different Er(III) ions, such a difference would be, if any, very small as the $O_{carboxylate}$–Er bond distances remain very similar. Hence, the hypothesis that the presence of two maxima in the χ''_M vs. T plot for compound **10** is due to the disordered hydrogen bond should be taken with caution. The temperature dependence of χ''_M at each frequency was fitted to the generalized Debye model in the range of 2.0–4.8 K, obtaining the relaxation times at different temperatures. The linear portion of the data was fitted to the Arrhenius law obtaining $U_{eff} = 24.0$ K with $\tau_0 = 1.19 \times 10^{-7}$ s (Fig. S30†).

It is worth mentioning that the distribution of donor atoms and Dy-donor distances in the Dy(III) ion coordination environment plays an essential role in determining the SMM behaviour. In this regard, low symmetry Dy(III) complexes generally exhibit an axial ground state (with a large contribution of $m_J = \pm 15/2$ to its wave function), which is required for the SMM behaviour. This axial ground state has an oblate disc shaped electron density distribution and can be stabilized by an axial crystal field,[5a,28] which can be generated when: (i) one of the Dy–O bond distances in the Dy(III) coordination sphere is very short and much shorter than the other Dy–O distances[29] and (ii) the donor atoms involved in the shortest Dy–O bonds are located at both sides of the Dy(III) ion.[9] In both cases, to reduce the repulsive interactions between the donor atoms with the largest electron densities (those possessing the shortest Dy–O distances) and the oblate (disc) electron density of the axial ground state, this disc is placed perpendicular to the shortest Dy–O bonds.[29] As a result, the magnetic moment, that is perpendicular to the electron density disc, is situated in the direction of the shortest Dy–O bonds. For the Er(III) complexes, an equatorial crystal field is needed to obtain an axial ground

state and SMM behaviour, as the electron density of this state possesses a prolate shape.

Taking into account the above considerations, for the dinuclear Zn(II)–Ln(III) complexes **1–6** and **9–10**, with Dy–O bond distances in their coordination spheres that are found in a short range, the crystal field can be considered as intermediate between axial and equatorial and therefore, the absence of SMM at zero field is not unexpected. The fact that in some cases the Dy(III) complexes present field-induced SMM behaviour with a larger thermal energy barrier than the Er(III) counterparts, whereas in other cases the opposite behaviour is observed, depends on the specific crystal field created by the donor atoms (if it is closer to an axial or to equatorial field). For the tetranuclear Zn_2Dy_2 complex **7**, there exists on each Dy(III) ion a Dy–O bond distance (2.213 Å and 2.255 Å) that is much shorter than the other ones (>0.1 Å, even though 3 methanol molecules are released after filtration, the tetranuclear core is well preserved and the Dy–O bond lengths will not be affected significantly). In this coordination environment, an almost pure axial ground state is expected for each Dy(III) ion, where the anisotropy axes are located along the direction of the shorter Dy–O distances.[29] This orientation of the magnetic moments has been confirmed using the Chilton's electrostatic model (Fig. S42†).[30] Despite the expected axiality for the ground state in complex **7**, it does not exhibit SMM behaviour, which can be due to the existence of weak exchange interactions between the Dy(III) ions through the alkoxo-bridging group, which are known to favour fast QTM relaxation. In this case, the weak Dy⋯Dy interaction destroys the barrier to magnetization reversal because the anisotropy axis of Dy(III) is not completely parallel between them and with the line connecting the Dy(III) ions.[31]

Luminescence properties

The solid state photoluminescence spectra were recorded for polycrystalline samples of all compounds since they contain Dy(III) and Er(III) ions that could provide lanthanide centred emissions in the visible and NIR ranges, respectively. It should be noted that lanthanide-based PL emitters have proven very useful not only in applications related to solid-state lighting such as the development of organic light-emitting diodes, flat panel displays or luminescent thermometers,[13,32] but also in the area of medical imaging and optical communication technologies, as they are frequently employed as fluoroimmunoassays.[33] A major advantage of these luminophores lies on their sharp and significantly long-lived emission that allows discriminating it from background fluorescence.[34] However, the emission efficiency of these systems is determined by their light absorption capacity, which usually demands indirect excitation of ligands to surpass the inherent low absorption coefficients of internal f–f transitions in lanthanide(III) ions (through the well-known "antenna effect"). Taking into account that the whole PL process is largely affected by the vibrational quenching of the molecular matrix in which lanthanide(III) ions are enclosed, the measurements were performed at 10 K to avoid thermally activated non-radiative pro-

cesses.[35] Steady-state emission spectra of Dy-based compounds (**1**, **3**, **5**, **7** and **9**) were recorded at 340 nm excitation (Fig. 6). All spectra share the occurrence of a broad band centred at 460 nm that may be attributed to the emission of organic ligands, whereas the characteristic emission bands corresponding to the Dy(III) ion are comparatively less intense. In particular, the bands sited at 482 and 575 nm, assigned to $^4F_{9/2} \rightarrow {}^6H_{15/2}$ and $^4F_{9/2} \rightarrow {}^6H_{13/2}$ transitions, respectively, are clearly distinguished for **1**, **7** and **9**, whereas they are substantially weak for **3** and **5** (that of 482 nm is in fact embedded within the main band). It is worth noticing that only for compound **7** both Dy-based transitions are of the same intensity, as it is commonly observed for most Dy(III) containing organic polymers.[36]

Accordingly, given that all measurements have been accomplished under the same physical conditions, it can be stated that the intensity of the Dy-based PL emission follows the **7** > **9** ≈ **1** > **3** ≈ **5** trend. In view of the emission profiles and the latter trend, it can be concluded that there is a weak ligand-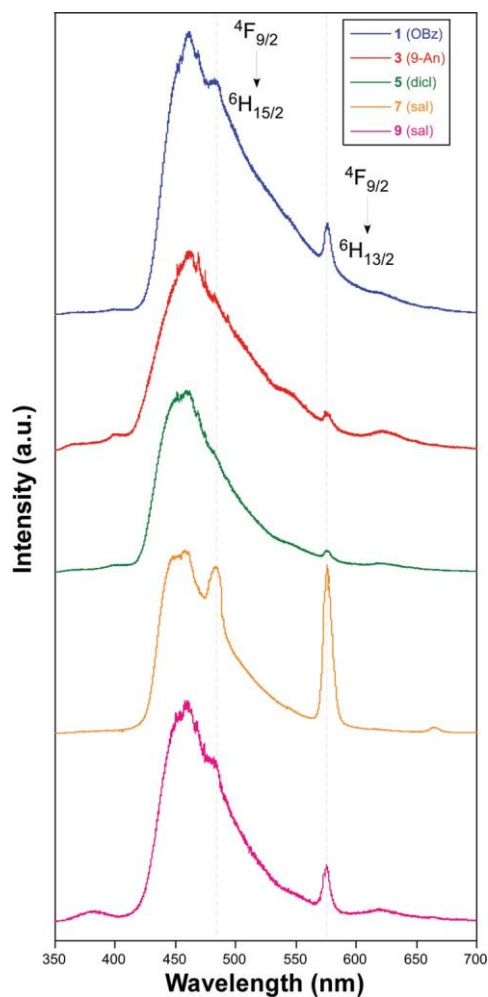to-metal charge transfer (antenna effect) in most of the compounds. The excitation spectra were recorded in all cases fixing the characteristic $^4F_{9/2} \rightarrow {}^6H_{15/2}$ emission line at 482 nm (see Fig. S43†). As inferred from them, excitation bands show the maxima close to the selected 340 nm wavelength except for compound **3**, in which a second and much more intense excitation is observed peaking at 430 nm. The higher wavelength excitation seems to be related to the π–π* transitions occurring on the 9-anthracenecarboxylate ligand in agreement with previous studies.[37] With the aim of exploring the efficiency of the An → Dy(III) charge transfer, the emission spectrum of **3** was also measured under 425 nm excitation (Fig. 7). The latter spectrum contains a narrow band with the main emission centred at 483 nm, which fits well the wavelength of the $^4F_{9/2} \rightarrow {}^6H_{15/2}$ transition, meaning that the An ligand is able to sensitize Dy(III) atoms more efficiently than L^{2-}. In any case, given the great sensitization capacity shown by the salicylate bridge, we decided to check the evolution of the emission spectra of compound **7** according to the temperature (see Fig. S44†). Upon heating the sample, it is observed that Dy(III) centred emission loses progressively intensity, while the corresponding bands (at 483 and 575 nm) get broadened in such a way that a poor Dy(III) centred emission is inferred from the spectrum at 300 K. This effect derives from the increase of the kinetic (thermal) energy of the bond electrons.[38]

On another level, emission spectra were recorded at 10 K for compounds **2**, **4**, **6**, **8** and **10** under a monochromatic laser at 325 nm (Fig. 8). Despite the fact that emissions in the NIR are often quenched by molecular vibrations even at low temperature,[39] these ligands are capable of transferring the excitation energy to erbium(III) ions, which could be potentially
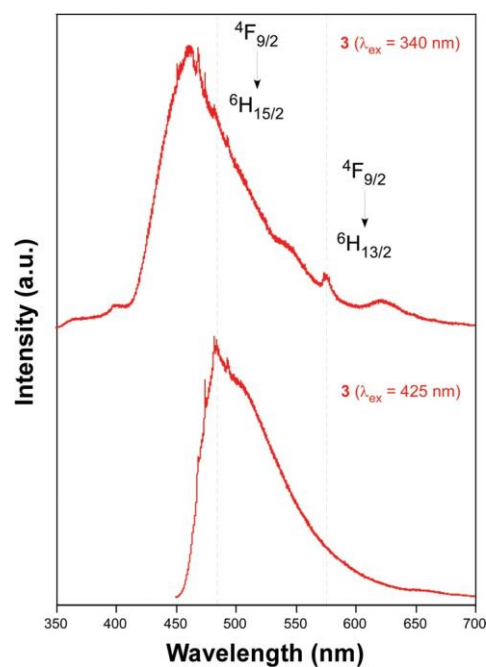

Fig. 6 Emission spectra of compounds **1**, **3**, **5**, **7** and **9** under λ_{ex} = 340 nm.

Fig. 7 Comparative emission of compound **3** under variable excitation wavelengths.
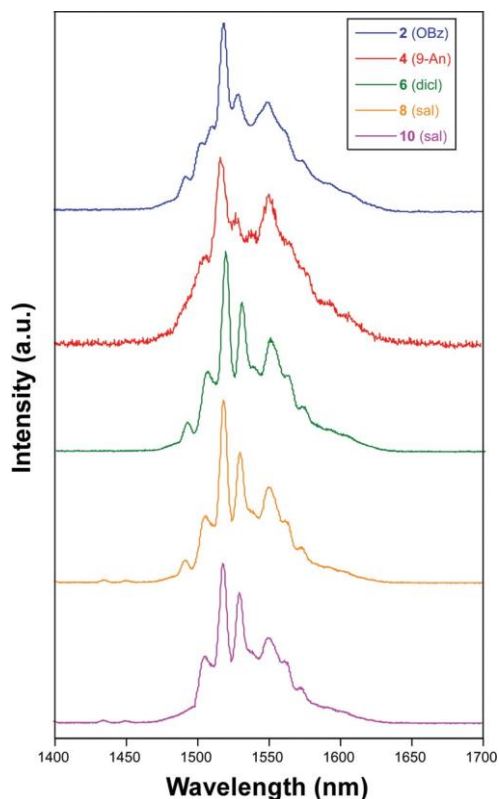
Fig. 8 Emission spectra of compounds **2**, **4**, **6**, and **8** under λ_{ex} = 325 nm.

Fig. 9 Fitted decay curves for compounds **1** and **2** under λ_{ex} = 325 nm.

Table 2 Best fitting results for lanthanide(III) centred emission decay curves of compounds **1**–**10**

$^4F_{9/2} \rightarrow {}^6H_{15/2}[Dy(III)]$			$^4I_{13/2} \rightarrow {}^4I_{15/2}[Er(III)]$		
Compound	τ (μs)	χ^2	Compound	τ (ns)	χ^2
1	3.3(6)	1.247	**2**	695(3)	1.314
3	3.2(5)	1.302	**4**	780(7)	1.321
5	3.1(5)	1.240	**6**	790(8)	1.366
7	3.2(5)	1.198	**8**	690(4)	1.311
9	3.0(3)	1.219	**10**	750(4)	1.225

taking place through a Förster's mechanism where the energy transfer proceeds from excited ligand levels to resonant levels of more energetic inner levels of the lanthanide.[40] All spectra share the presence of a sharp and structured multiplet centred at 1540 nm that corresponds to the $^4I_{13/2} \rightarrow {}^4I_{15/2}$ transition of the intraionic levels of the Er(III) ion, which is an appropriate wavelength in the third telecommunication window of common erbium-doped fibre amplifiers.[41] A comparative analysis of all spectra on the basis of their relative intensity reveals that emission capacity fits the **8** ≈ **10** ≈ **6** > **2** > **4**. This trend confirms that the salicylate ligand provides the most efficient charge transfer to both lanthanide centres, a fact that should be originated at the small energy gap between the triplet state of the salicylate ligand in the complexes and the emissive level (or their overtones) of the lanthanide(III) centres.[35] On the other hand, though a quantitative comparison between these emission spectra and those of Dy(III)-based compounds cannot be performed, based on the strong signal of the emission band it may be stated that lanthanide-centred emission is nearly of the same order.

In order to gain deeper insights into the PL performance of both luminophores, decay curves were recorded at $^4F_{9/2} \rightarrow {}^6H_{15/2}$ and $^4I_{13/2} \rightarrow {}^4I_{15/2}$ emission lines, respectively for Dy-based and Er-based compounds. At first glance, all compounds showed very similar curves that were successfully fitted using a single-exponential function $[I_t = A_0 + A_1 \exp(-t/\tau)]$
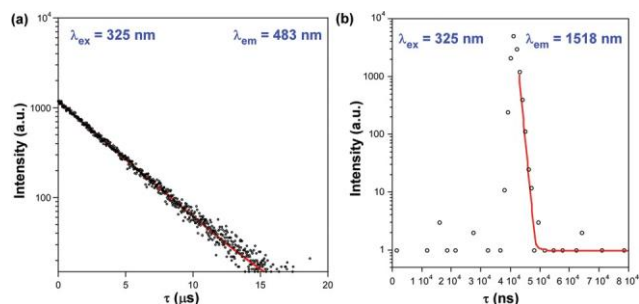
(Fig. 9). Uniform lifetimes of *ca.* 3 μs and 700 ns are accordingly estimated irrespective of the selected emission wavelength for Dy-based and Er-based complexes (Table 2 and Fig. S45 and S46†). The measured values are somewhat short and fit within the range of those previously reported for other lanthanide(III)-based coordination compounds.[36,42] Therefore, these measurements raise their interest for some abovementioned specific applications in which short emissions are needed in response to the light stimulus.

Conclusions

The reaction between the *N,N′*-dimethyl-*N,N′*-bis(2-hydroxy-3-formyl-5-bromobenzyl)ethylenediamine compartmental ligand (H₂L), the corresponding Ln(NO₃)₃·nH₂O and Zn(NO₃)₂·4H₂O salts and the respective ancillary carboxylate bridging ligand (benzoate, anthracenate, diclofenac, salicylate, 2,6-dihydroxybenzoate) led to eleven new ZnLn complexes. Nine of them (compounds **1–6**, **10–11**) display dinuclear ZnLn structures, whilst complexes **7** and **8** are tetranuclear Zn₂Ln₂ complexes. The acidic character of the salicylic acid ancillary ligand, which in the presence of methanol causes the methoxylation of the H₂L ligand yielding a hemiacetal H₃L′, promotes the assembly of two tetranuclear ZnLn units to afford the Zn₂Ln₂ entity.

Magnetic properties showed that SMM behaviour of the complexes is not only affected by the type of Ln(III) ion but also by the carboxylate bridging ligand connecting the Zn(II) and Ln(III) ions. Compounds **3** and **10** showed two maxima in the χ''_M *vs.* T plot, which may be justified by a direct relaxation process in the former and by the presence of a disordered

phenol group of the salicylate ligand in the latter. This disorder can lead to two Er(III) ions with different electronic density depending on the position of the phenol group. Good supporting evidence of this hypothesis could be the fact that compound **11** (in which the disorder is not possible because the phenol groups of the 2,6-dihydroxybenzoate ancillary bridging ligand form simultaneously two hydrogen bonds with the carboxylate oxygen atoms) exhibits only a maximum in the χ''_M *vs. T* plot. Nevertheless, the above justifications should be taken with caution as two maxima can also appear for non-disordered structures possessing only equivalent Ln(III) ions. Moreover, very similar Ln(III) ions, to those observed for the disordered phenol group in compound **11**, would lead to nearly identical dynamic relaxation processes which would be difficult to recognize.

Photoluminescence properties of the obtained compounds showed that the ligands have the ability to sensitize lanthanide centred emissions in the visible and near-infrared regions with variable capacity. Overall, a similar trend is observed for Dy(III) and Er(III) based compounds, which confirms that the salicylate ligand provides the most efficient charge transfer to both lanthanide centres, a fact that seems to be related to the small energy gap between the triplet state of the ligand and the emissive level of the lanthanide(III) centres.

Conflicts of interest

There are no conflicts to declare.

Acknowledgements

Notes and references

1 D. Gatteschi, R. Sessoli and J. Villain, *Molecular Nanomagnets*, Oxford University Press, Oxford, U.K., 2006.

2 (*a*) A. R. Rocha, V. M. García-Suárez, S. W. Bailey, C. J. Lambert, J. Ferrerand and S. Sanvito, *Nat. Mater.*, 2005, 4, 335; (*b*) M. Affronte, *J. Mater. Chem.*, 2009, 19, 1731.

3 (*a*) L. Bogani and W. Wernsdorfer, *Nat. Mater.*, 2008, 7, 179; (*b*) R. Vincent, S. Klyatskaya, M. Ruben, W. Wernsdorfer and F. Balestro, *Nature*, 2012, 488, 357; (*c*) M. Ganzhorn, S. Klyatskaya, M. Ruben and W. Wernsdorfer, *Nat.*

Nanotechnol., 2013, 8, 165; (*d*) M. Jenkins, T. Hümmer, M. J. Marínez-Pérez, J. García-Ripoll, D. Zueco and F. Luis, *New J. Phys.*, 2013, 15, 095007.

4 (*a*) M. N. Leuenberger and D. Loss, *Nature*, 2001, 410, 789; (*b*) A. Ardavan, O. Rival, J. L. Morton, S. J. Blundell, A. M. Tyryshkin, G. A. Timco and R. E. P. Winpenny, *Phys. Rev. Lett.*, 2007, 98, 057201; (*c*) P. C. E. Stampand and A. Gaita-Ariño, *J. Mater. Chem.*, 2009, 19, 1718; (*d*) M. J. Martínez-Pérez, S. Cardona-Serra, C. Schlegel, F. Moro, P. J. Alonso, H. Prima-García, J. M. Clemente-Juan, M. Evangelisti, A. Gaita-Ariño, J. Sesé, J. Van Slageren, E. Coronado and F. Luis, *Phys. Rev. Lett.*, 2012, 108, 247213.

5 (*a*) R. A. Layfield and M. Murugesu, *Lanthanides and Actinides in Molecular Magnetism*, Wiley-VCH, Weinheim, Germany, 2015; (*b*) J. D. Rinehart and J. R. Long, *Chem. Sci.*, 2011, 2, 2078; (*c*) Y. N. Guo, G. F. Xu, Y. Guo and J. Tang, *Dalton Trans.*, 2011, 40, 9953; (*d*) L. Sorace, C. Benelli and D. Gatteschi, *Chem. Soc. Rev.*, 2011, 40, 3092; (*e*) J. Luzon and R. Sessoli, *Dalton Trans.*, 2012, 41, 13556; (*f*) J. M. Clemente-Juan, E. Coronado and A. Gaita-Ariño, *Chem. Soc. Rev.*, 2012, 41, 7464; (*g*) D. N. Woodruff, R. E. P. Winpenny and R. A. Layfield, *Chem. Rev.*, 2013, 113, 5110; (*h*) P. Zhang, Y.-N. Guo and J. Tang, *Coord. Chem. Rev.*, 2013, 257, 1728.

6 Y.-S. Ding, N. F. Chilton, R. E. P. Winpenny andY.-Z. Zheng, *Angew. Chem., Int. Ed.*, 2016, 55, 16071.

7 C. A. P. Goodwin, F. Ortu, D. Reta, N. F. Chilton and D. P. Mills, *Nature*, 2017, 548, 439.

8 A. Upadhyay, S. K. Singh, C. Das, R. Mondol, S. K. Langley, K. S. Murray, G. Rajaraman and M. Shanmugam, *Chem. Commun.*, 2014, 50, 8838.

9 (*a*) I. Oyarzabal, J. Ruiz, J. M. Seco, M. Evangelisti, A. Camón, E. Ruiz, D. Aravena and E. Colacio, *Chem. – Eur. J.*, 2014, 20, 14262; (*b*) I. Oyarzabal, J. Ruiz, E. Ruiz, D. Aravena, J. M. Seco and E. Colacio, *Chem. Commun.*, 2015, 51, 12353; (*c*) I. Oyarzabal, A. Rodríguez-Diéguez, M. Barquín, J. M. Seco and E. Colacio, *Dalton Trans.*, 2017, 46, 4278.

10 I. Oyarzabal, B. Artetxe, A. Rodríguez-Diéguez, J. A. García, J. M. Seco and E. Colacio, *Dalton Trans.*, 2016, 45, 9712.

11 (*a*) R. A. Bulman, in *Metal Ions in Biological Systems*, ed. A. Sigel and H. Sigel, Marcel Dekker Inc., New York, 2003, ch. 17, vol. 40; (*b*) S. V. Eliseeva and J. C. Bünzli, *Chem. Soc. Rev.*, 2010, 39, 189; (*c*) C. H. Evans, *Biochemistry of the Lanthanides*, Plenum Press, New York, 1990.

12 (*a*) S. Comby and J.-C. G. Bünzli, in *Handbook on the Physics and Chemistry of Rare Earths*, ed. K. A. Gschneidner Jr, J.-C. G. Bünzli and V. K. Pecharsky, Elsevier Science B.V., Amsterdam, 2007, ch. 235, vol. 37; (*b*) F. Wang and X. Liu, *Chem. Soc. Rev.*, 2009, 38, 976.

13 J. Rocha, C. D. S. Brites and L. D. Carlos, *Chem. – Eur. J.*, 2016, 22, 14782.

14 (*a*) J. C. G. Bünzli, *Chem. Rev.*, 2010, 110, 2729; (*b*) S. Faulkner, S. J. A. Pope and B. P. Burton-Pye, *Appl. Spectrosc. Rev.*, 2005, 40, 1; (*c*) S. Lin, *Chem. Soc. Rev.*, 2004, 33, 445.

15 M. Yonemura, Y. Matsumura, M. Ohba, H. Okawa and D. E. Fenton, *Chem. Lett.*, 1996, 601.

16 *CrysAlisPro Software System*, Agilent Technologies UK Ltd, Oxford, UK, 2012.

17 *Bruker Apex2*, Bruker AXS Inc., Madison, Wisconsin, USA, 2004.

18 G. M. Sheldrick, *SADABS, Program for Empirical Adsorption Correction*, Institute for Inorganic Chemistry, University of Gottingen, Germany, 1996.

19 G. M. Sheldrick, *SHELXTL Version 2014/7*, http://shelx.uni-ac.gwdg.de/SHELX/index.

20 A. L. Spek, *Acta Crystallogr., Sect. D: Biol. Crystallogr.*, 2009, 65, 148.

21 D. Klein, *Organic Chemistry*, Wiley, 3rd edn, 2016.

22 K. Manseki, H. Sakiyama, M. Sakamoto, Y. Nishida, H. Aono, Y. Sadaoka, M. Ohba and H. Okawa, *Synth. React. Inorg. Met.-Org. Chem.*, 2001, 31, 1443.

23 M. Llunell, D. Casanova, J. Cirera, J. M. Bofill, P. Alemany, S. Alvarez, M. Pinsky and D. Avnir, *SHAPE, v1.1b*, Barcelona, Spain, 2005.

24 N. F. Chilton, *CCFIT program*, The Chilton Group, Manchester, U.K., 2014, http://www.nfchilton.com/software.html.

25 C. Shi, R. Nie, X. Yao, S. Fan, G. An, Y. Dong and G. Li, *RSC Adv.*, 2017, 7, 49701.

26 (*a*) J. Ruiz, A. J. Mota, A. Rodríguez-Diéguez, S. Titos, J. M. Herrera, E. Ruiz, E. Cremades, J. P. Costes and E. Colacio, *Chem. Commun.*, 2012, 48, 7916; (*b*) S. Das, A. Dey, S. Biswas, E. Colacio and V. Chandrasekhar, *Inorg. Chem.*, 2014, 53, 3417.

27 (*a*) B. Liu, B.-W. Wang, Z.-M. Wang and S. Gao, *Sci. China: Chem.*, 2012, 55, 926; (*b*) A. Arauzo, A. Lazarescu, S. Shova, E. Bartolomé, R. Cases, J. Luzón, J. Bartolomé and C. Turta, *Dalton Trans.*, 2014, 43, 12342; (*c*) H. X. Zhang, S. Y. Lin, S. F. Xue, C. Wang and J. K. Tang, *Dalton Trans.*, 2015, 44, 4648.

28 (*a*) T. Kajiwara, M. K. Nakano, S. Takaishi and M. Yamashita, *Chem. − Eur. J.*, 2011, 17, 196; (*b*) A. Watanabe, A. Yamashita, M. Nakano, T. Yamamura and T. Kajiwara, *Chem. − Eur. J.*, 2011, 17, 7428.

29 (*a*) D. Aravena and E. Ruiz, *Inorg. Chem.*, 2013, 52, 13770; (*b*) M. M. Hänninen, A. J. Mota, D. Aravena, E. Ruiz, R. Sillanpää, A. Camón, M. Evangelisti and E. Colacio, *Chem. − Eur. J.*, 2014, 20, 8410; (*c*) J. P. Costes, S. Titos-Padilla, I. Oyarzabal, T. Gupta, C. Duhayon, G. Rajaraman and E. Colacio, *Inorg. Chem.*, 2016, 55, 4428.

30 N. F. Chilton, D. Collison, E. J. L. McInnes, R. E. P. Winpenny and A. Soncini, *Nat. Commun.*, 2013, 4, 2551.

31 E. Moreno Pineda, N. F. Chilton, R. Marx, M. Dörfel, D. O. Sells, P. Neugebauer, S. D. Jiang, D. Collison, J. van Slageren, E. J. McInnes and R. E. Winpenny, *Nat. Commun.*, 2014, 5, 5243.

32 (*a*) W.-J. Yang, L. Luo, T.-M. Chen and N.-S. Wang, *Chem. Mater.*, 2005, 17, 3883; (*b*) T. Kinoshita, M. Yamazaki, H. Kawazoe and H. Hosono, *J. Appl. Phys.*, 1999, 86, 3729; (*c*) R. C. Evans, P. Douglas and C. J. Winscom, *Coord. Chem. Rev.*, 2006, 250, 2093; (*d*) W. P. Lustig, S. Mukherjee, N. D. Rudd, A. V. Desai, J. Li and S. K. Ghosh, *Chem. Soc. Rev.*, 2017, 46, 3242.

33 (*a*) I. Hemmilä, *J. Alloys Compd.*, 1995, 225, 480; (*b*) J. Moynagh and H. Schimmel, *Nature*, 1999, 400, 105.

34 (*a*) M. Albrecht, O. Osetska, R. Frohlich, J. C. G. Bünzli, A. Aebischer, F. Gumy and J. Hamacek, *J. Am. Chem. Soc.*, 2007, 129, 14178; (*b*) S. Banerjee, L. Huebner, M. D. Romanelli, G. A. Kumar, R. E. Riman, T. J. Emge and J. G. Brennan, *J. Am. Chem. Soc.*, 2005, 127, 15900; (*c*) J. C. G. Bünzli, *Acc. Chem. Res.*, 2006, 39, 53; (*d*) J. C. G. Bünzli and C. Piguet, *Chem. Soc. Rev.*, 2005, 34, 1048; (*e*) M. D. Ward, *Coord. Chem. Rev.*, 2007, 251, 1663.

35 (*a*) S. V. Elisseva, D. N. Pleshkov, K. A. Lyssenko, L. S. Lepnev, J. C. Bünzli and N. P. Kuzmina, *Inorg. Chem.*, 2010, 49, 9300; (*b*) A. de Bettencourt-Dias, P. S. Barber, S. Viswanathan, D. T. de Lill, A. Rollett, G. Ling and S. Altun, *Inorg. Chem.*, 2010, 49, 8848.

36 (*a*) S. Quici, M. Cavazzini, G. Marzanni, G. Accorsi, N. Armaroli, B. Ventura and F. Barigelletti, *Inorg. Chem.*, 2005, 44, 529; (*b*) Y. L. Gai, K.-C. Xiong, L. Chen, Y. Bu, X.-J. Li, F.-L. Jiang and M.-C. Hong, *Inorg. Chem.*, 2012, 51, 13128; (*c*) I. Oyarzabal, B. Fernández, J. Cepeda, S. Gómez-Ruiz, A. J. Calahorro, J. M. Seco and A. Rodríguez-Diéguez, *CrystEngComm*, 2016, 18, 3055.

37 (*a*) M. A. Palacios, S. Titos-Padilla, J. Ruiz, J. M. Herrera, S. J. A. Pope, E. K. Brechin and E. Colacio, *Inorg. Chem.*, 2014, 53, 1465; (*b*) B. Branchi, P. Ceroni, V. Balzani, F. G. Klaerner and F. Voegtle, *Chem. − Eur. J.*, 2010, 16, 6048.

38 J. Cepeda, S. Pérez-Yáñez, G. Beobide, O. Castillo, J. A. García, M. Lanchas and A. Luque, *Dalton Trans.*, 2015, 44, 6972.

39 W. M. Yen, S. Shionoya and H. Yamamoto, in *Phosphor Handbook*, CRC Press, Athens, 2007.

40 (*a*) N. M. Shavaleev, G. Accorsi, D. Virgili, Z. R. Bell, T. Lazarides, G. Calogero, N. Armaroli and M. D. Ward, *Inorg. Chem.*, 2005, 44, 61; (*b*) T. Förster, *Discuss. Faraday Soc.*, 1959, 27, 7.

41 (*a*) L. N. Sun, H. J. Zhang, L. S. Fu, F. Y. Liu, Q. G. Meng, C. Y. Peng and J. B. Yu, *Adv. Funct. Mater.*, 2005, 15, 1041; (*b*) S. Dang, J.-B. Yu, X.-F. Wang, Z.-Y. Guo, L.-N. Sun, R.-P. Deng, J. Feng, W.-Q. Fan and H.-J. Zhang, *J. Photochem. Photobiol., A*, 2010, 214, 152.

42 (*a*) J. M. Seco, I. Oyarzabal, S. Pérez-Yáñez, J. Cepeda and A. Rodríguez-Diéguez, *Inorg. Chem.*, 2016, 55, 11230; (*b*) R. G. Sun, Y. Z. Wang, Q. B. Zheng, H. J. Zhang and A. J. Epstein, *J. Appl. Phys.*, 2000, 87, 7589; (*c*) A. Zabala-Lekuona, J. Cepeda, I. Oyarzabal, A. Rodríguez-Diéguez, J. A. García, J. M. Seco and E. Colacio, *CrystEngComm*, 2017, 19, 256; (*d*) K. Kuriki, Y. Koike and Y. Okamoto, *Chem. Rev.*, 2002, 102, 2347.